

The optical variability of steep-spectrum radio quasars in the SDSS Stripe 82 region

Minfeng Gu¹ and Y. L. Ai^{2,3}

¹ Key Laboratory for Research in Galaxies and Cosmology, Shanghai Astronomical Observatory, Chinese Academy of Sciences, 80 Nandan Road, Shanghai 200030, China

e-mail: gumf@shao.ac.cn

² National Astronomical Observatories/Yunnan Observatory, Chinese Academy of Sciences, P.O. Box 110, 650011 Kunming, Yunnan, China

³ Key Laboratory for the Structure and Evolution of Celestial Objects, Chinese Academy of Sciences, P.O. Box 110, 650011 Kunming, Yunnan, China

Preprint online version: August 4, 2011

ABSTRACT

Context. While there are a lot of investigations on the optical variability of flat-spectrum radio quasars (FSRQs), not much work has been done on the optical variability of steep-spectrum radio quasars (SSRQs).

Aims. We investigate the optical variability in SSRQs. For comparison, the optical variability of FSRQs are also explored.

Methods. We investigate the optical variability of 18 SSRQs and 15 FSRQs in the SDSS Stripe 82 region using SDSS DR7 released multi-epoch data covering about nine years. We determined the spectral index by fitting a powerlaw to SDSS *ugriz* photometric data, and explored the relationship between the spectral index and source brightness.

Results. For all SSRQs studied, we detect variations in *r* band flux of overall amplitude between 0.22 mag and 0.92 mag in different sources. Eight of 18 SSRQs display a bluer-when-brighter (BWB) trend. In contrast, the variability amplitude of 15 FSRQs in *r* band ranges from 0.18 to 0.97 mag, and 11 of 15 sources show a BWB trend. We found an anti-correlation between the Eddington ratio and the variability amplitude in *r* band for SSRQs, which is similar to that in radio quiet AGNs. This implies that the thermal emission from accretion disk may be responsible for the variability in SSRQs, although the jet nonthermal emission cannot be excluded. In contrast, there is no correlation in FSRQs, which implies that the mechanisms of variability in FSRQs may be different from that in SSRQs. The optical continuum variability of radio loud broad absorption line quasars (BALQs) are investigated for the first time here on two sources with steep radio spectrum. Both radio loud BALQs show variations with amplitude of about 0.3 mag at *r* band. Their spectral variability all show a BWB trend. In a combined sample (18 SSRQs, and 44 FSRQs) of our sample with the FSRQs in Gu & Ai (2011), we found a trend of a broader line width of broad Mg II emission line with steeper radio spectral index. It implies a disc-like broad line region (BLR) geometry may present in these quasars. In these 62 quasars, we found a $\sim 57\%$ source percentage showing BWB trend in FSRQs, whereas it is $\sim 44\%$ in SSRQs.

Key words. galaxies: active – galaxies: quasars: general – galaxies: photometry

1. Introduction

Active galactic nuclei (AGNs) are characteristic of variability at almost all wavelength (e.g. Wiita 1996). Multiwavelength studies of variations of AGNs have played important roles in exploring the physical conditions near the center of AGNs. Based on the variability, the reverberation mapping method was developed to calculate the size of broad line region (BLR). From the photoionization model, the flux variations of BLR follows the flux variation of continuum ionization emission with certain time lag, which corresponds to the size of BLR (Peterson 1993). Moreover, the disc-jet connections can be investigated by using the long term multiwavelength variability monitorings (e.g. Chatterjee et al. 2009, 2011).

Intrinsically, the variations of AGNs are generally caused by the physical variations in jet and accretion disc. However, the contribution of each component in the observed variability varies from source to source. Blazars, including BL Lac objects and flat-spectrum radio quasars (FSRQs), are the most extreme class of active galactic nuclei (AGNs), characterized by strong and rapid variability, high polarization, and apparent superluminal motion. These extreme properties are generally in-

terpreted as a consequence of non-thermal emission from a relativistic jet oriented close to the line of sight. In general, the variations in blazars are dominated by the jet emission. There are extensive explorations on the optical variability of blazars (e.g. Ghisellini et al. 1997; Fan et al. 1998; Massaro et al. 1998; Ghosh et al. 2000; Clements & Carini 2001; Raiteri et al. 2001; Villata et al. 2002; Vagnetti et al. 2003; Wu et al. 2005, 2007; Gu et al. 2006; Hu et al. 2006; Poon et al. 2009; Rani et al. 2010; Gu & Ai 2011). While it is generally accepted that the nonthermal emission from relativistic jet oriented close to the line of sight dominate the optical continuum, the situation seems more complicated in FSRQs. It is not clear whether the nonthermal jet emission plays the main role in the optical variability. Evidence of thermal emission in FSRQs has been detected in several cases usually during low activity states (e.g. 3C279, Pian et al. 1999; 3C273, Grandi & Palumbo 2004; 3C454.3, Raiteri et al. 2007). A recent work shows that the optical variability in the FSRQ PKS 1510-089 is mainly due to the thermal emission, and only during major flares a contribution from the jet is seen (D’Ammando et al. 2011). Moreover, the redder-when-brighter trend found in several FSRQs implies that the thermal emission

plays important role in the optical variability (e.g. Gu et al. 2006; Rani et al. 2010; Gu & Ai 2011).

Radio-quiet AGNs has also been explored in terms of the long-term or short-term variability (e.g. Stalin et al. 2004, 2005; Gupta & Joshi 2005; Ai et al. 2010). The accretion disc instabilities may likely explain the optical microvariability in radio quiet AGNs (e.g. Gopal-Krishna et al. 1995, see also Gopal-Krishna et al. 2003 for alternative scenario). In terms of the long-term variability, the change of accretion rate is used to explain the optical variations in radio quiet AGNs (e.g. Li & Cao 2008). The properties of steep spectrum radio quasars (SSRQs) are intermediate between FSRQs and radio quiet quasars. SSRQs are usually lobe-dominated radio quasars, with radio lobe emission dominate over the radio core emission. Their jets are viewed at larger angles than blazars. Therefore, the beaming effects from jets should not be severe (see e.g. Liu et al. 2006), and the jet emission is not expected to dominate at optical bands (e.g. Gu & Ai 2011). However, the variations in SSRQs could still be a mixture of being caused by jet and accretion disc, since they are powerful radio emitter. The optical variations of SSRQs are largely unknown, and there are only few explorations on variations in SSRQs (e.g. Stalin et al. 2004, 2005). While the color variations and/or spectral variations of blazars are extensively investigated (e.g. Ghisellini et al. 1997; Fan et al. 1998; Massaro et al. 1998; Ghosh et al. 2000; Clements & Carini 2001; Raiteri et al. 2001; Villata et al. 2002; Vagnetti et al. 2003; Wu et al. 2005, 2007; Gu et al. 2006; Rani et al. 2010; Gu & Ai 2011), it has rarely been done for SSRQs. In this work, we investigate the optical variability for a sample of SSRQs, as well as their spectral variations.

The layout of this paper is as follows: in Section 2, we describe the source sample; the variability results are outlined in Section 3; Section 4 includes the discussion; and in the last section, we draw our conclusions. The cosmological parameters $H_0 = 70 \text{ km s}^{-1} \text{ Mpc}^{-1}$, $\Omega_m = 0.3$, and $\Omega_\Lambda = 0.7$ are used throughout the paper, and the spectral index α is defined as $f_\nu \propto \nu^{-\alpha}$, where f_ν is the flux density at frequency ν .

2. Sample selection

2.1. Quasars in Stripe 82 region

Our initial quasar sample was selected as those quasars both in the SDSS DR7 quasar catalogue (Schneider et al. 2010) and Stripe 82 region. The SDSS DR7 quasar catalogue consists of 105,783 spectroscopically confirmed quasars with luminosities brighter than $M_i = -22.0$, with at least one emission line having a full width at half-maximum (FWHM) larger than 1000 km s^{-1} and highly reliable redshifts. The sky coverage of the sample is about 9380 deg^2 and the redshifts range from 0.065 to 5.46. The five-band (u, g, r, i, z) magnitudes have typical errors of about 0.03 mag. The spectra cover the wavelength range from 3800 to 9200 \AA with a resolution of ≈ 2000 (see Schneider et al. 2010 for details). The Stripe 82 region, i.e. right ascension $\alpha = 20^{\text{h}} - 4^{\text{h}}$ and declination $\delta = -1^{\circ}.25 - +1^{\circ}.25$, was repeatedly scanned during the SDSS-I phase (2000 - 2005) under generally photometric conditions, and the data are well calibrated (Lupton et al. 2002). This region was also scanned repeatedly over the course of three 3-month campaigns in three successive years in 2005 - 2007 known as the SDSS Supernova Survey (SN survey). The multi-epoch photometric observations therefore enable us to investigate the optical variability of the selected quasars.

2.2. Cross-correlation with radio catalogues

In this paper, we define a quasar to be a SSRQ according to its radio spectral index. Therefore, we cross-correlate the initial quasar sample with the Faint Images of the Radio Sky at Twenty centimeters (FIRST) 1.4-GHz radio catalogue (Becker, White & Helfand 1995), the Green Bank 6-cm (GB6) survey at 4.85 GHz radio catalogue (Gregory et al. 1996), and the Parkes-MIT-NRAO (PMN) radio continuum survey at 4.85 GHz (Griffith & Wright, 1993), as well as for sources with $\delta < 0^\circ$. The FIRST survey used the Very Large Array (VLA) to observe the sky at 20 cm (1.4 GHz) with a beam size of 5.4 arcsec. FIRST was designed to cover the same region of the sky as the SDSS, and observed 9000 deg^2 at the north Galactic cap and a smaller $2^\circ.5$ wide strip along the celestial equator. It is 95 per cent complete to 2 mJy and 80 per cent complete to the survey limit of 1 mJy. The survey contains over 800,000 unique sources, with an astrometric uncertainty of $\lesssim 1 \text{ arcsec}$.

The GB6 survey at 4.85 GHz was executed with the 91-m Green Bank telescope in 1986 November and 1987 October. Data from both epochs were assembled into a survey covering the $0^\circ < \delta < 75^\circ$ sky down to a limiting flux of 18 mJy, with 3.5 arcmin resolution. GB6 contains over 75,000 sources, and has a positional uncertainty of about 10 arcsec at the bright end and about 50 arcsec for faint sources (Kimball & Ivezić 2008). The PMN surveys were made using the Parkes 64-m radio telescope at a frequency of 4850 MHz with the NRAO multibeam receiver mounted at the prime focus (Griffith & Wright 1993). The surveys had a spatial resolution of approximately $4'.2$ FWHM and were made for the southern sky between declinations of -87° and $+10^\circ$, and all right ascensions during June and November in 1990. The positional accuracy is close to 10 arcsec in each coordinate. The survey was divided into four declination bands. One of these four is the equatorial survey ($-9^\circ.5 < \delta < +10^\circ.0$) covering 1.90 sr , which contains 11,774 sources to a flux limit of 40 mJy and largely overlaps the GB6 survey in the declination range from 0° to $+10^\circ$ (Griffith et al. 1995).

The initial quasar sample was first cross-correlated between the SDSS quasar positions and the FIRST catalogue to within 2 arcsec (see e.g. Ivezić et al. 2002; Lu et al. 2007). The resulting sample of SDSS quasar positions was then cross-correlated with both the GB6 and PMN equatorial catalogues to within 1 arcmin (e.g. Kimball & Ivezić 2008). Owing to the different spatial resolutions of FIRST, GB6, and PMN, multiple FIRST counterparts were found to within 1 arcmin for some quasars, although there is only single GB6 and/or PMN counterpart existed. The optical variability of quasars with single FIRST counterparts to within 1 arcmin of the SDSS positions has been presented in Gu & Ai (2011). In this paper, we focus on the optical variability of quasars with multiple FIRST counterparts.

There are total 29 sources having multi FIRST counterparts within 1 arcmin of SDSS positions. The radio spectral index α_r was then calculated between the integrated FIRST 1.4 GHz from multi-counterparts within 1 arcmin and either or both of the GB6 and PMN 4.85 GHz. Eleven sources are defined as SSRQs with $\alpha_r > 0.5$ using the integrated 1.4 GHz flux density. In comparison, only two sources are defined as SSRQs if only using 1.4 GHz flux density of the closest counterpart. This implies that most genuine SSRQs may appear as multi-FIRST components, but be identified as FSRQs if using the flux density of the closest FIRST component, which is actually much smaller than that of radio lobes. When counterparts were found in both the GB6 and PMN surveys, the spectral indices were consistent with each other. To further check the spectral index, we searched for the

counterparts in NRAO VLA Sky Survey (NVSS) within 1 arcmin of SDSS positions. The NVSS was also carried out using the VLA at 1.4 GHz to survey the entire sky north of $\delta = -40^\circ$ and contains over 1.8 million unique detections brighter than 2.5 mJy, however with lower spatial resolution $45'' \text{beam}^{-1}$. Due to the lower spatial resolution, all sources have single NVSS counterpart, except for five sources, which have two counterparts, i.e. SDSS J015105.80-003426.4, SDSS J213513.10-005243.8, SDSS J221409.96+005227.0, SDSS J220719.77+004157.3, and SDSS J233624.04+000246.0. We then re-calculated the spectral index using the flux density from single or integrated NVSS counterparts. We found that 25 out of 29 sources have consistent spectral index between using FIRST and NVSS. Three sources (SDSS J005905.51+000651.6, SDSS J013352.66+011345.1 and SDSS J021225.56+010056.1) changed from FSRQs to SSRQs using NVSS flux density, for which the part of emission can be likely missed in FIRST images. One source, i.e. SDSS J015509.00+011522.5, changes from steep to flat spectral index, but the spectral index are all close to 0.5. Therefore, it is still treated as SSRQ. Among the 29 sources, 14 are defined as SSRQs with $\alpha_r \geq 0.5$, whereas 15 objects are FSRQs with $\alpha_r < 0.5$ (see Table 1).

2.3. Sample

For completeness, in the following analysis we include five SSRQs of Gu & Ai (2011), and the resulting sample consists of 19 SSRQs. This sample of 19 SSRQs is listed in Table 1, which provides the source redshift, radio loudness, radio spectral index, black hole mass, disc bolometric luminosity, and the Eddington ratio. The same parameters relative to the 15 FSRQs are listed as a comparison. The distribution of redshift, radio loudness, black hole mass, and the Eddington ratio are shown in Fig. 1. We found that SSRQs are more extended in the distribution of each parameters than FSRQs. The source redshift is taken directly from the SDSS DR7 quasar catalogue, which covers $0.17 < z < 2.63$ for SSRQs, while $0.34 < z < 2.00$ for FSRQs. The radio loudness is from Shen et al. (2011), which ranges from $\log R = 1.80$ (SDSS J013352.66+011345.1) to $\log R = 5.00$ (SDSS J000622.60-000424.4) for SSRQs, whereas it is 1.55 - 3.54 for FSRQs. However, the radio loudness was calculated as $R = f_{6\text{cm}}/f_{2500}$, where $f_{6\text{cm}}$ and f_{2500} are the flux density at rest-frame 6 cm and 2500Å, respectively (see Shen et al. 2011 for more details). Among 15 FSRQs, 4 sources have an inverted spectral index between 1.4 and 4.85 GHz with $\alpha_r < 0$.

Black hole masses are estimated from the various empirical relations in the literature by using the luminosity and FWHM of broad H β , Mg II, and C IV lines, i.e., Vestergaard & Peterson (2006) for H β , and Kong et al. (2006) for Mg II and C IV. The luminosity and FWHM of broad H β , Mg II, and C IV lines are adopted from the measurements in Shen et al. (2011). The BLR luminosity L_{BLR} is derived following Celotti, Padovani & Ghisellini (1997) by scaling the strong broad emission lines H β , Mg II, and C IV to the quasar template spectrum of Francis et al. (1991), in which Ly α is used as a flux reference of 100. By adding the contribution of H α with a value of 77, the total relative BLR flux is 555.77, which consists of H β at 22, Mg II at 34 and C IV at 63 (Francis et al. 1991; Celotti et al. 1997). From the BLR luminosity, we estimate the disc bolometric luminosity as $L_{\text{Bol}} = 10L_{\text{BLR}}$ (Netzer 1990). It can be seen from Table 1 and Fig. 1 that the black hole mass of SSRQs ranges from $10^{8.29} M_\odot$ to $10^{10.08} M_\odot$ for SSRQs, while $10^{8.44} M_\odot$ to $10^{9.56} M_\odot$ for FSRQs.

The Eddington ratio of SSRQs $\log L_{\text{Bol}}/L_{\text{Edd}}$ ranges from -2.35 to 0.52, while in FSRQs it ranges from -2.03 to 0.30.

3. Results

The SDSS DR7 CAS contains the Stripe82 database, containing all imaging from SDSS stripe 82 along the celestial equator at the southern Galactic cap. It includes a total of 303 runs, covering any given piece of the close to 270 deg² area approximately 80 times. Only about one-quarter of the stripe 82 scans were obtained in photometric conditions, the remainder being taken under variable clouds and often poorer than normal seeing. For the runs that were non-photometric, an approximate calibration, using the photometric frames as reference, was derived and made available in the CAS Stripe82 database. In this work, we directly use the point-spread-function magnitudes in the CAS Stripe82 database from the photometric data obtained during the SDSS-I phase from data release 7 (DR7; Abazajian et al. 2009) and the SN survey during 2005 - 2007. The typical measurement error in magnitude is about 0.03 mag.

Among 19 SSRQs, we select the sources classified as point sources in all observational runs. Only data with good measurements (high-quality photometry) are selected following the recommendations in the SDSS instructions¹. Moreover, we insist on the *ugriz* magnitude being brighter than the magnitude limit in each band, i.e. 22.0, 22.2, 22.2, 21.3, 20.5 at *u*, *g*, *r*, *i*, *z*, respectively. The data taken at cloudy conditions are also excluded. We calculate the spectral index α_r from the linear fit to the $\log f_\nu - \log \nu$ relation after applying an extinction correction to the *ugriz* flux density and taking the flux error into account. In most cases, the linear fit gave good fits. Each cycle of *ugriz* photometry was usually completed within five minutes, i.e. quasi-simultaneously, therefore, the spectral index calculation will not be seriously influenced by any source variations.

3.1. SSRQs

3.1.1. Variability

Among 19 SSRQs, SDSS J013352.66+011345.1 was excluded from our analysis owing to the low quality of the photometric data. All remaining 18 SSRQs show large amplitude variations with overall variations in *r* band $\Delta r = 0.22 - 0.92$ mag (see Table 1). In general, the variations in different bands show similar trends.

The correlation between the spectral index α_r and PSF *r* magnitude was checked for all sources using the Spearman rank correlation analysis method. We found that 8 of 18 SSRQs show a significant positive correlation at a confidence level of $> 99\%$. The positive correlation indicates that the source spectrum becomes flatter when the source is brighter. The result shows that a bluer-when-brighter trend is clearly detected in these eight SSRQs.

3.1.2. Broad Absorption Line Quasars

Among the 18 SSRQs, we found that two sources are defined as broad absorption line quasar (BALQ) in the literature. SDSS J024534.07+010813.7 ($z = 1.5363$) was listed as a BALQ in Gibson et al. (2009) selected from SDSS DR5. This source is also included in the First Bright Quasar Survey with name of FBQS J0245+0108 (Becker et al. 2001). It appears as a single

¹ <http://www.sdss.org/dr7/products/catalogs/flags.html>

counterpart in the NVSS within 1 arcmin of SDSS position with a flux density of $f_{\text{NVSS}} = 337.9$ mJy and position angle of 55.5 degree. However, it has three counterparts in the FIRST within 1 arcmin of SDSS positions (see Fig. 2). Three counterparts align with a similar position angle with that of NVSS counterpart. This difference is simply caused by the different spatial resolution of FIRST and NVSS in the case that the radio structure can be resolved in former, however not in the latter. The flux density of the closest FIRST counterpart is 11.67 mJy, while the integrated flux density of all counterparts is $f_{\text{FIRST}} = 317.2$ mJy. Therefore, the radio emission of this source is highly dominated by the large scale double radio lobes. The spectral index calculated for the integrated FIRST 1.4 GHz and PMN 4.85 GHz flux density of $f_{\text{PMN}} = 115$ mJy is $\alpha_r = 1.05$, while it is $\alpha_r = 0.82$ when the GB6 4.85 GHz flux density of $f_{\text{GB6}} = 85.7$ mJy is used. In contrast, the spectral index will be highly inverted if only the flux density of the closest FIRST counterpart is used.

The light curves of SDSS J024534.07+010813.7 in u, g, r, i, and z bands are shown in Fig. 3. The variations exhibit similar trends in all bands, over seven years from 2000 to 2007. The overall variation in r band is 0.29 mag. In the observational sessions, the source became gradually fainter from 2000 to 2004, and then stayed quite stable from 2004 to 2007.

In SDSS J024534.07+010813.7, a significant positive correlation present between the spectral index α_r and r magnitude, which is shown in Fig. 4. The Spearman correlation analysis shows a significant positive correlation with a correlation coefficient of $r_s = 0.435$ at confidence level of $> 99.9\%$. The positive correlation shows that the source spectrum becomes flatter when the source is brighter, i.e. that there is a bluer-when-brighter trend. With the source redshift $z = 1.5363$, SDSS *ugriz* wavebands correspond to the wavelength range of 1400–3521 Å in the source rest-frame. For a sample of 17 radio-quiet AGNs, Shang et al. (2005) show that the spectral break occurs at around 1100 Å for most objects, which is thought to be closely related to the big blue bump. If this spectral break also exists in SDSS J024534.07+010813.7, we would expect to observe the rising part of accretion disk thermal emission when it dominates over the nonthermal emission. However, the spectral index in the observational sessions are in the range of 1.59 to 2.03. This implies a falling SEDs in the rest frame 1400–3521 Å. This can be likely caused by the internal extinction in quasar itself, for example, from the outflowing absorption gas.

We found another BALQ SDSS J021728.62–005227.2 ($z = 2.4621$) in SSRQs of Gu & Ai (2011). It is defined as BALQ in Trump et al. (2006) selected from SDSS DR3. It is defined as SSRQs in Gu & Ai (2011) with radio spectral index of $\alpha_r = 0.75$. Its overall variations amplitude in r band is $\Delta r = 0.35$. The significant positive correlation between the r magnitude and the optical spectral index shows a bluer-when-brighter trend in this source. However, unlike SDSS J024534.07+010813.7, the spectral index varies from 0.45 to 1.28, with most time staying at < 1.0 . The internal extinction from the outflowing absorption gas may not be severe in this source.

3.2. FSRQs

All 15 FSRQs show large amplitude variations with overall variations in r band $\Delta r = 0.18 - 0.97$ (see Table 1). The correlation between the spectral index α_r and PSF r magnitude was checked for all sources using the Spearman rank correlation analysis method. We found that 11 of 15 FSRQs show a sig-

nificant positive correlation at a confidence level of $> 99\%$, i.e. a bluer-when-brighter trend.

3.3. BLR geometry

Assuming the radio spectral index as an indicator of orientation, the BLR geometry can be investigated when line width of broad emission lines are included (Fine et al. 2011). To this end, we combine all sources in this work and those FSRQs in Gu & Ai (2011), resulting a sample of 62 quasars, which includes 18 SSRQs and 44 FSRQs. The relationship between the radio spectral index and FWHM of Mg II line is shown in Fig. 5 for a subsample of 55 sources (42 FSRQs and 13 SSRQs) with available Mg II line measurements. There is a trend of broader Mg II lines with steeper spectral index. The Spearman rank correlation analysis shows a positive correlation with correlation coefficient of $r_s = 0.298$ at confidence level of 97.3%. The mean value of Mg II FWHM is 4075 km s⁻¹ for FSRQs, while it is 6110 km s⁻¹ for SSRQs. The median value of Mg II FWHM is 3586 km s⁻¹ and 5694 km s⁻¹ for FSRQs and SSRQs, respectively. Although our sample is much smaller than theirs, the results are consistent with that of Fine et al. (2011), which used the radio spectral index between Westerbork Northern Sky Survey 330 MHz and NVSS 1.4 GHz. The result implies a disk-like BLR geometry may present in these quasars.

4. Discussions

4.1. SSRQs and FSRQs

While FSRQs are usually associated with core-dominated radio quasars, SSRQs are generally related to lobe-dominated ones, usually with two large-scale optically thin radio lobes. Usually, the beaming effect is not severe in SSRQs because of the relatively large viewing angle. Therefore, the optical continuum of SSRQs could be dominated by the thermal emission. In Fig. 6, most SSRQs with available Mg II measurements lie close to or below the solid line for radio quiet AGNs. The average value of the ratio of the luminosity at 3000 Å to that of broad Mg II line is $< \log (vL_{\nu}(3000\text{\AA})/L_{\text{MgII}}) > = 1.78 \pm 0.26$, which is in good agreement with the linear relation for radio quiet AGNs (see Fig. 6). This likely implies that the thermal emission from accretion disk is indeed the dominant one in the optical continuum at the epoch of SDSS spectra for most SSRQs, if not all. For comparison, 14 FSRQs with Mg II measurements are also plotted in Fig. 6. We found that the distribution of FSRQs are generally similar to that of SSRQs, but with larger scatter. The average value of the ratio of the luminosity at 3000 Å to that of broad Mg II line is $< \log (vL_{\nu}(3000\text{\AA})/L_{\text{MgII}}) > = 1.81 \pm 0.31$, which is slightly larger than that of SSRQs. This may imply that the optical non-thermal jet emission may not be dominant in all FSRQs, as found by Chen et al. (2009).

Interestingly, eight of 18 SSRQs display a BWB trend (see Table 1). The BWB trend has also been found in radio quiet AGNs, and the variability was found to be anti-correlated with the Eddington ratio (Ai et al. 2010). In radio quiet AGNs, the optical variability could be due to the variation in the accretion process, for example, the variation in the accretion rate (e.g. Li & Cao 2008), since the jet is either weak or absent. These explanations could also be used to explain the variability of SSRQs if the optical emission is indeed mainly from the accretion disk. To further investigate the mechanism of variability in SSRQs, the relationship between the variability Δr and the Eddington ratio is plotted in Fig. 7. We found an anti-correlation

with a Spearman correlation coefficient of $r_s = -0.490$ at confidence level of 96.2%. This similar anti-correlation to radio quiet AGNs, strongly implies that the mechanisms of optical variability may be similar in the two populations. The thermal emission from the accretion disk may be responsible for the variability of SSRQs. In contrast, there is no correlation for FSRQs. This implies that the mechanism of variability in FSRQs may be different from that of SSRQs. However, that the variation in SSRQs is caused by jet nonthermal emission cannot be completely excluded in some cases because the variability amplitudes are generally larger than the typical values for radio quiet AGNs, 0.05 - 0.3 mag (e.g. Ai et al. 2010), (see Table 1). In extreme cases, the overall amplitude is $\Delta r = 0.92$ mag in SDSS J013514.39–000703.8. It may be more likely that both thermal and nonthermal emission contribute to the variability. Further multi-waveband monitoring is needed to help resolve these uncertainties, especially the spectroscopic monitoring.

In terms of optical variability on month-to-year time-scales, no obvious difference was found in the behavior of radio quiet quasars and lobe-dominated quasars (LDQs) (Stalin et al. 2004). Moreover, there is no significant difference in either the amplitude or duty cycle of intranight optical variability (INOV) between these two classes of non-blazar AGNs. However, their sample is too small, and the time spanned by observations is too short. Nevertheless, the authors infer that the radio loudness of a quasar alone is not a sufficient condition for a pronounced INOV. While the observational data cannot exclude accretion disc flares as the source of the intranight optical variability in radio quiet quasars and LDQs, it does not preclude a substantial contribution from blazar-like relativistically beamed emission. As suggested by Stalin et al. (2005), the radio quiet quasars may also eject relativistic jets. However, their jets are probably quenched while crossing the innermost micro-arcsecond scale, possibly through heavy inverse Compton losses in the vicinity of the central engine (e.g. Gopal-Krishna et al. 2003). However, the analysis of spectra of a set of radio quiet quasars that had already been searched for microvariability showed that the jet-based scenario is unlikely (Chand, Wiita & Gupta 2010).

In order to compare systematically the variations of SSRQs with FSRQs, we combine the FSRQs of Gu & Ai (2011) with sources in this work. The combined sample consists of 62 quasars, of which 44 are FSRQs, and 18 are SSRQs. We show the histogram of variation amplitude in r band Δr for both SSRQs and FSRQs in Fig. 8. It can be seen that Δr of FSRQs are systematically larger than that of SSRQs, with median value of 0.52 mag and 0.41 mag for FSRQs and SSRQs, respectively. Apparently, FSRQs cover wider range in Δr . Four FSRQs exhibit $\Delta r > 1.0$ mag with an extreme case of $\Delta r = 3.46$ (see Gu & Ai 2011), while none in SSRQs. This implies that the variations in FSRQs are systematically more violent than SSRQs. This is most likely due to the relativistic jet, which is viewed at smaller viewing angle in FSRQs. The fact that the typical variations amplitude of SSRQs is between the values of radio quiet AGNs and FSRQs is qualitatively consistent with the source nature of SSRQs, which are radio-loud sources with prominent powerful relativistic jets, however viewed at larger viewing angle resulting in a dominated thermal emission at optical wavebands. In terms of the spectral variations, eight of 18 SSRQs show BWB trend at confidence level of $> 99\%$, i.e. at probability of $\sim 44\%$. In contrast, 25 ($\sim 57\%$) of the 44 FSRQs show BWB trend at confidence level of $> 99\%$, while only one source shows a RWB trend at confidence level of $> 99\%$. Therefore, it seems that BWB trend are quite common both in FSRQs and in SSRQs, although the mechanisms can be different, for example, shock-in-

jet and accretion rate change are mainly responsible for FSRQs and SSRQs, respectively.

In the unification scheme of AGNs, the radio galaxies are generally unified with radio quasars (Antonucci 1993), with radio galaxies being viewed at large viewing angle. The jet emission in radio galaxies are not severely boosted, then the dominated optical emission is expected to be thermal emission related to the accretion disk. Indeed, it is argued that the optical and X-ray emission arise from the accretion disk - corona system in two radio galaxies 3C 120 and 3C 111 by using extensive multi-frequency monitoring data (Chatterjee et al. 2009, 2011). In both sources, the low optical polarization supports the thermal origin of the optical emission. However, in 3C 111 the detection of polarization percentages of 3% or even higher suggests that during particular activity phases an additional contribution from non-thermal emission from the jet may be present (Jorstad et al. 2007; Chatterjee et al. 2011). Interestingly, significant dips in the X-ray light curve are followed by ejections of bright superluminal knots in the VLBA images for both sources. The authors argued that the radiative state of accretion disk plus corona system, where the X-rays are produced, has a direct effect on the events in the jet, where the radio emission originates.

Similar to many FSRQs in Gu & Ai (2011) having a spectral index $\alpha_\nu < 1.0$, almost all FSRQs in this work show $\alpha_\nu < 1.0$, implying a rising SED in optical regions. One possibility is that the optical emission is mainly from thermal accretion disc, although these sources are defined as FSRQs. Alternatively, they can be high-synchrotron-peaked FSRQs, since the synchrotron peak frequency is higher than the rest-frame frequency of SDSS *ugriz* wavebands. This however needs further investigations.

4.2. BALQs

The nature of BAL quasars is still unclear. It was argued that the outflowing BAL wind is preferentially equatorial, and only in those objects with almost edge-on accretion disk to the line of sight, can be observed as BAL (Cohen et al. 1995; Goodrich & Miller 1995). However, the VLBI radio images of BALQs argued against this orientation scenario, in terms of the radio structures and both the steep and flat radio spectrum (e.g. Jiang & Wang 2003; Liu et al. 2008; Doi et al. 2009). Fine et al. (2011) found no evidence that BAL QSOs have a different spectral index distribution to non-BALs although only 25 obvious BALs are considered in their sample. Their BALQs both have steep and flat radio spectrum computed using the Westerbork Northern Sky Survey (WENSS) at 330 MHz and the NVSS at 1.4 GHz. In general, the radio-loud BALQs tend to be compact in the radio, similar to Gigahertz-Peaked Spectrum (GPS) and Compact Steep Spectrum (CSS) sources, which are thought to be at the young stage of large scale radio sources (Becker et al. 2000; Montenegro-Montes et al. 2009). It has been proposed that the BALs are not closely related with the inclinations, and may be associated with a relatively short-lived evolutionary phase with a large BAL wind covering fraction (e.g. Briggs et al. 1984; Gregg et al. 2000). We found that the two radio-loud steep spectrum BALQs in this paper have different radio structures. SDSS J024534.07+010813.7 has prominent extended double radio lobes, of which the emission dominates over that of radio core (see Fig. 2). The source is too extended (~ 52 arcsec, i.e. ~ 440 kpc) to be considered as a CSS/GPS. This source has not been imaged with VLBI. In contrast, SDSS J021728.62–005227.2 is compact in FIRST image with only single counterpart found. It has been imaged with VLBI by Doi et al. (2009). However, only a compact component was found

with flux density at 8.4 GHz $f_{8.4\text{GHz}} = 43$ mJy at scale of < 1 kpc. In combination with the FIRST flux density, the radio spectrum is steep $\alpha_r = 0.9$, which makes this source resemble to CSS, thus likely being a young radio source. More radio observations at higher spatial resolution would be helpful to better understand the nature of this source.

While there are many investigations on the variability of broad absorption line troughs (e.g. Barlow 1993; Lundgren et al. 2007; Gibson et al. 2008, 2010; Capellupo et al. 2011), not much works have been done on the optical continuum variability for BALQs. On timescales of the order of years, the optical continuum variability of BALQs was found to differ markedly from that of non-BAL radio quiet quasars (Turnshek 1988). In short timescales, intranight optical variations of $\sim 5\% - 9\%$ were detected on timescales of ~ 1 hr in two BALQs (Anupama & Chokshi 1998). The recent search for optical microvariability in a sample of 19 radio quiet BALQs argued that radio quiet BALQs do not appear to be a special case of the radio quiet quasars in terms of their similar duty cycle (Joshi et al. 2011). However, all these observations focused only on the radio quiet BALQs. Therefore, for the first time, we present here the optical continuum variability for radio loud BALQs, although only two sources are found in our sample. In both BALQs, the C IV BAL troughs fall outside the *ugriz* bands. Together with the similar trends of variability in different wavebands rule out the possibility of the observed light-curve variations being caused by variations in the strength of the BAL features. The variation amplitude in the *r* band of two sources is not atypical in overall sample of SSRQs, although they are at the low end of distribution in Fig. 8. This implies that the mechanism of optical continuum variability of radio-loud BALQs may likely be similar to that of more general SSRQs. Interestingly, both BALQs show BWB trend. The percentage of BWB trend is higher than that of SSRQs. However, the small sample size precludes to draw any firm conclusions. Certainly, a larger sample is needed for further investigations. The spectral index of two BALQs in this work are steeper than the typical value of other SSRQs, which implies more reddened in BALQs than non-BALQs. This is consistent with previous results (Trump et al. 2006; Gibson et al. 2009).

5. Summary

We have constructed a sample of 19 SSRQs and 15 FSRQs in the SDSS Stripe 82 region. The variability and the relationship between the spectral index and brightness were investigated for 18 SSRQs and 15 FSRQs. We found that all SSRQs show large-amplitude overall variations, e.g. from 0.22 to 0.92 mag in *r* band. We found a bluer-when-brighter trend in 8 of the 18 SSRQs studied here. In contrast, the variability amplitude of 15 FSRQs in *r* band ranges from 0.18 to 0.97 mag, and 11 of 15 sources show a BWB trend. We found an anti-correlation between the Eddington ratio and the variability amplitude in *r* band for SSRQs, which is similar to that in radio quiet AGNs. This implies that the thermal emission from accretion disk may be responsible for the variability in SSRQs, although the jet nonthermal emission cannot be excluded. In contrast, there is no correlation in FSRQs, which implies that the mechanisms of variability in FSRQs may be different from that in SSRQs. The optical continuum variability of radio loud BALQs is investigated for the first time here on two sources with steep radio spectrum. Both radio loud BALQs show variations with amplitude of about 0.3 mag at *r* band. Their spectral variability all show a bluer-when-brighter trend. In combination with 29 FSRQs also selected from Stripe 82 region in Gu & Ai (2011), we found a

trend of a broader line width of broad Mg II line with steeper radio spectral index. This implies a disc-like BLR geometry may present in these quasars. In these 62 quasars, we found a $\sim 57\%$ source percentage showing BWB trend in FSRQs, whereas it is $\sim 44\%$ in SSRQs.

Acknowledgements. We thank the anonymous referee for constructive comments that improved the manuscript. MFG thanks X. Cao, S. Li, A. Gupta, J. Wu and Z. Chen for useful discussions. This work is supported by the National Science Foundation of China (grants 10703009, 10821302, 10833002, 10978009, 11033007 and 11073039), and by the 973 Program (No. 2009CB824800). Funding for the SDSS and SDSS-II was provided by the Alfred P. Sloan Foundation, the Participating Institutions, the National Science Foundation, the U.S. Department of Energy, the National Aeronautics and Space Administration, the Japanese Monbukagakusho, the Max Planck Society, and the Higher Education Funding Council for England. The SDSS Web site is <http://www.sdss.org/>.

References

- Abazajian, K. N., Adelman-McCarthy, J. K., Agüeros, M. A., et al. 2009, *ApJS*, 182, 543
- Ai, Y. L., Yuan, W., Zhou, H. Y., et al. 2010, *ApJ*, 716, L31
- Antonucci, R. 1993, *ARA&A*, 31, 473
- Anupama, G. C., & Chokshi, A. 1998, *ApJ*, 494, L147
- Barlow, T. A., 1993, PhD thesis, Univ. California, San Diego
- Becker, R. H., White, R. L., & Helfand, D. J. 1995, *ApJ*, 450, 559
- Becker, R. H., White, R. L., Gregg, M. D., et al. 2000, *ApJ*, 538, 72
- Becker, R. H., White, R. L., Gregg, M. D., et al. 2001, *ApJS*, 135, 227
- Briggs, F. H., Turnshek, D. A., & Wolfe, A. M. 1984, *ApJ*, 287, 549
- Capellupo, D. M., Hamann, F., Shields, J. C., Rodríguez Hidalgo, P., & Barlow, T. A. 2011, *MNRAS*, 413, 908
- Celotti, A., Padovani, P., & Ghisellini, G., 1997, *MNRAS*, 286, 415
- Chand, H., Wiita, P. J., & Gupta, A. C. 2010, *MNRAS*, 402, 1059
- Chatterjee, R., Marscher, A. P., Jorstad, S. G., et al. 2009, *ApJ*, 704, 1689
- Chatterjee, R., Marscher, A. P., Jorstad, S. G., et al. 2011, *ApJ*, 734, 43
- Chen, Z. Y., Gu, M. F., & Cao, X. 2009, *MNRAS*, 397, 1713
- Clements, S. D., & Carini, M. T. 2001, *AJ*, 121, 90
- Cohen, M. H., Ogle, P. M., Tran, H. D., et al. 1995, *ApJ*, 448, L77
- D’Ammando, F., Raiteri, C. M., Villata, M., et al. 2011, *A&A*, 529, A145
- Doi, A., Kawaguchi, N., Kono, Y., et al. 2009, *PASJ*, 61, 1389
- Fan, J. H., Xie, G. Z., Pecontal, E., Pecontal, A., & Copin, Y. 1998, *ApJ*, 507, 173
- Fine, S., Jarvis, M. J., & Mauch, T. 2011, *MNRAS*, 412, 213
- Francis, P. J., Hewett, P. C., Foltz, C. B., et al. 1991, *ApJ*, 373, 465
- Ghisellini, G., Villata, M., Raiteri, C. M., et al. 1997, *A&A*, 327, 61
- Ghosh, K. K., Ramsey, B. D., Sadun, A. C., & Soundararajaperumal, S. 2000, *ApJS*, 127, 11
- Gibson, R. R., Brandt, W. N., Schneider, D. P., & Gallagher, S. C. 2008, *ApJ*, 675, 985
- Gibson, R. R., Jiang, L., Brandt, W. N., et al. 2009, *ApJ*, 692, 758
- Gibson, R. R., Brandt, W. N., Gallagher, S. C., Hewett, P. C., & Schneider, D. P. 2010, *ApJ*, 713, 220
- Goodrich, R. W., & Miller, J. S., 1995, *ApJ*, 448, L73
- Gopal-Krishna, Sagar, R., & Wiita, P. J. 1995, *MNRAS*, 274, 701
- Gopal-Krishna, Stalin, C. S., Sagar, R., & Wiita, P. J. 2003, *ApJ*, 586, L25
- Gregg, M. D., Becker, R. H., Brotherton, M. S., et al. 2000, *ApJ*, 544, 142
- Gregory, P. C., Scott, W. K., Douglas, K., & Condon, J. J. 1996, *ApJS*, 103, 427
- Grandi, P., & Palumbo, G. 2004, *Science*, 306, 998
- Griffith, M. R., & Wright, A. E. 1993, *AJ*, 105, 1666
- Griffith, M. R., Wright, A. E., Burke, B. F., & Ekers, R. D. 1995, *ApJS*, 97, 347
- Gu, M. F., Lee, C.-U., Pak, S., Yim, H. S., & Fletcher, A. B. 2006, *A&A*, 450, 39
- Gu, M. F., & Ai, Y. L. 2011, *A&A*, 528, A95
- Gupta, A. C., & Joshi, U. C. 2005, *A&A*, 440, 855
- Hu, S. M., Zhao, G., Guo, H. Y., Zhang, X., & Zheng, Y. G. 2006, *MNRAS*, 371, 1243
- Ivezić, Ž., Menou, K., Knapp, G. R., et al. 2002, *AJ*, 124, 2364
- Jiang, D. R., & Wang, T. G. 2003, *A&A*, 397, L13
- Jorstad, S. G., Marscher, A. P., Stevens, J. A., et al. 2007, *AJ*, 134, 799
- Joshi, R., Chand, H., Gupta, A. C., & Wiita, P. J. 2011, *MNRAS*, 412, 2717
- Kimball, A. E., & Ivezić, Ž. 2008, *AJ*, 136, 684
- Kong, M. Z., Wu, X. B., Wang, R., & Han, J. L. 2006, *Chinese J. Astron. Astrophys.*, 6, 396
- Li, S. L., & Cao, X. W. 2008, *MNRAS*, 387, L41
- Liu, Y., Jiang, D. R., & Gu, M. F. 2006, *ApJ*, 637, 669

- Liu, Y., Jiang, D. R., Wang, T. G., & Xie, F. G. 2008, *MNRAS*, 391, 246
- Lu, Y., Wang, T., Zhou, H., & Wu, J. 2007, *AJ*, 133, 1615
- Lundgren, B. F., Wilhite, B. C., Brunner, R. J., et al. 2007, *ApJ*, 656, 73
- Lupton, R. H., Ivezić, Ž., Gunn, J. E., et al. 2002, *Proc. SPIE*, 4836, 350
- Massaro, E., Nesci, R., Maesano, M., Montagni, F., & D'Alessio, F. 1998, *MNRAS*, 299, 47
- Montenegro-Montes, F. M., Mack, K.-H., Benn, C. R., et al. 2009, *Astron. Nachr.*, 330, 157
- Netzer, H. 1990 in *Active Galactic Nuclei*, ed. R. D. Blandford et al. (Berlin: Springer), 57
- Peterson, B. M. 1993, *PASP*, 105, 247
- Pian, E., Urry, C. M., Maraschi, L., et al. 1999, *ApJ*, 521, 112
- Poon, H., Fan, J. H., & Fu, J. N. 2009, *ApJS*, 185, 511
- Raiteri, C. M., Villata, M., Aller, H. D., et al. 2001, *A&A*, 377, 396
- Raiteri, C. M., Villata, M., Larionov, V. M., et al. 2007, *A&A*, 473, 819
- Rani, B., Gupta, A. C., Strigachev, A., et al. 2010, *MNRAS*, 404, 1992
- Schneider, D. P., Richards, G. T., Hall, P. B., et al. 2010, *AJ*, 139, 2360
- Shang, Z. H., Brotherton, M. S., Green, R. F., et al. 2005, *ApJ*, 619, 41
- Shen, Y., Richards, G. T., Strauss, M. A., et al. 2011, *ApJS*, 194, 45
- Stalin, C. S., Gopal-Krishna, Sagar, R., & Wiita, P. J. 2004, *MNRAS*, 350, 175
- Stalin, C. S., Gupta, A. C., Gopal-Krishna, Wiita, P. J., & Sagar, R. 2005, *MNRAS*, 356, 607
- Trump, J. R., Hall, P. B., Reichard, T. A., et al. 2006, *ApJS*, 165, 1
- Turnshek, D. A. 1988, in *QSO absorption lines: probing the Universe*, ed. J. C. Blades et al. (Cambridge), 17
- Vagnetti, F., Trevese, D., & Nesci, R. 2003, *ApJ*, 590, 123
- Vestergaard, M., & Peterson, B. M. 2006, *ApJ*, 641, 689
- Villata, M., Raiteri, C. M., Kurtanidze, O. M., et al. 2002, *A&A*, 390, 407
- Wiita, P. J., 1996, in *Miller H. R., Webb J. R., Noble J. C., eds, ASP Conf. Ser. Vol. 110, Blazar Continuum Variability. Astron. Soc. Pac., San Francisco*, 42
- Wu, J. H., Peng, B., Zhou, X., et al. 2005, *AJ*, 129, 1818
- Wu, J. H., Zhou, X., Ma, J., et al. 2007, *AJ*, 133, 1599

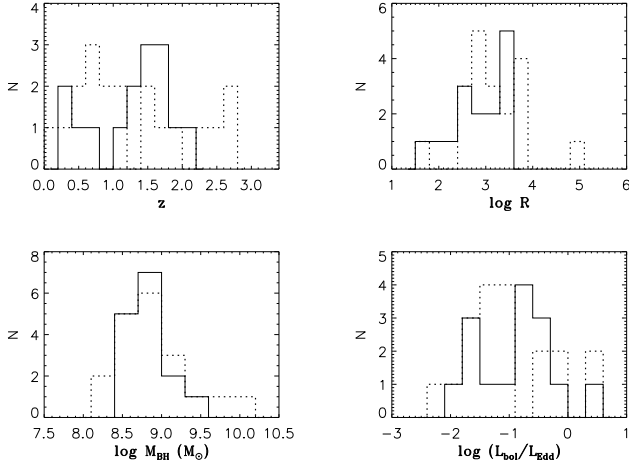


Fig. 1. The histogram of sample parameters: redshift (upper left), radio loudness (upper right), black hole mass (lower left), and the Eddington ratio (lower right). The dotted lines are for 19 SSRQs, and solid lines are for 15 FSRQs.

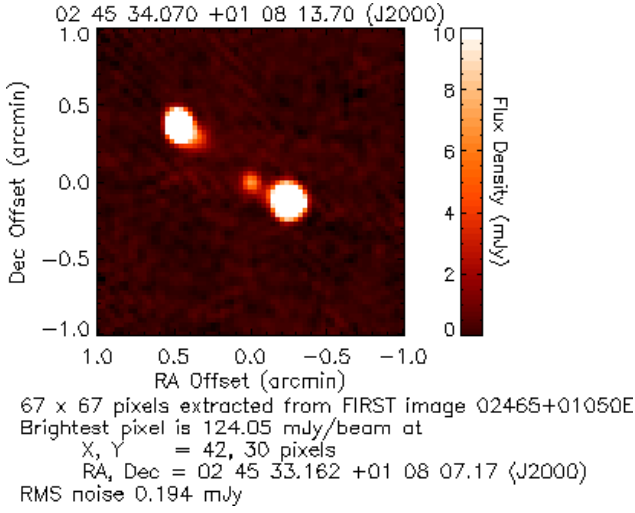


Fig. 2. The FIRST radio image of SDSS J024534.07+010813.7.

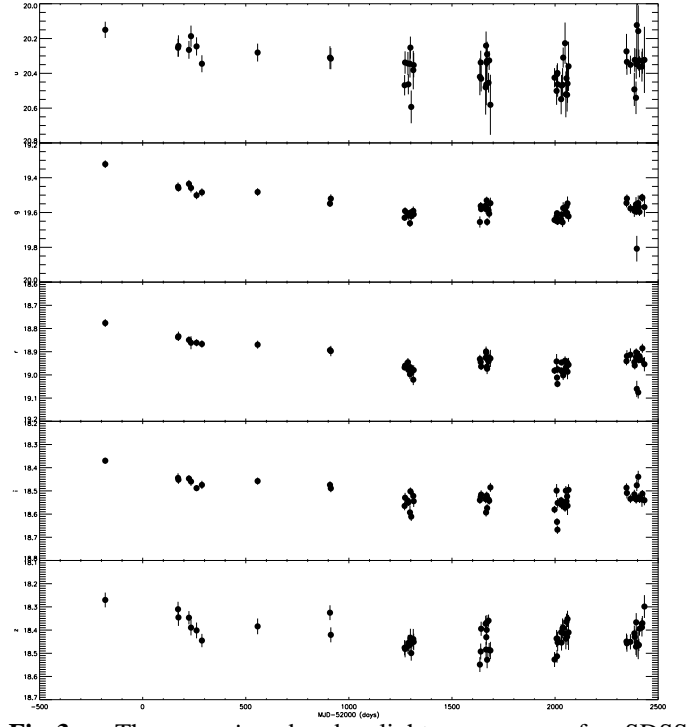


Fig. 3. The *ugriz* band light curve of SDSS J024534.07+010813.7 (from top to bottom).

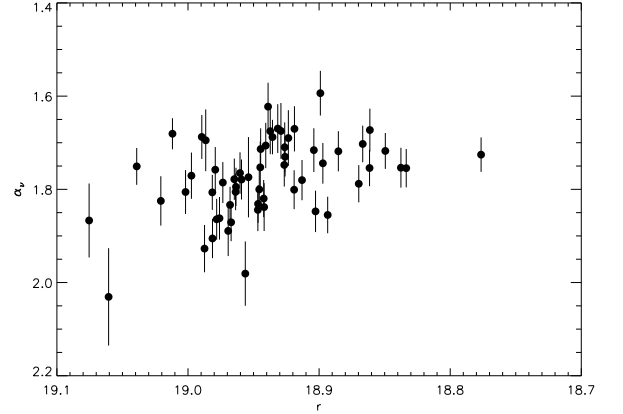


Fig. 4. The relationship between the spectral index and the PSF magnitude at *r* band for SDSS J024534.07+010813.7. A significant positive correlation is present, which implies a bluer-when-brighter trend.

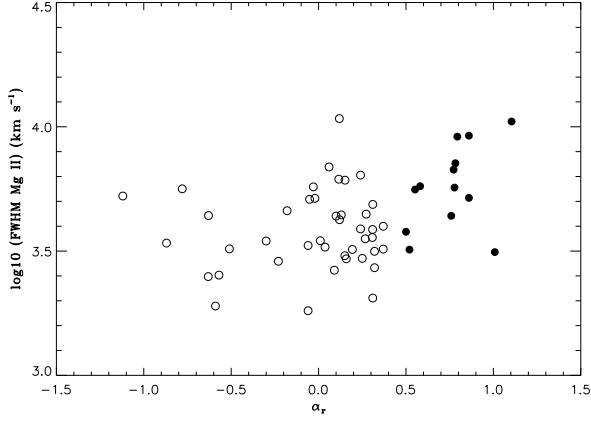


Fig. 5. The line width of broad Mg II line versus radio spectral index. The solid circles represent SSRQs, while the open circles are for FSRQs.

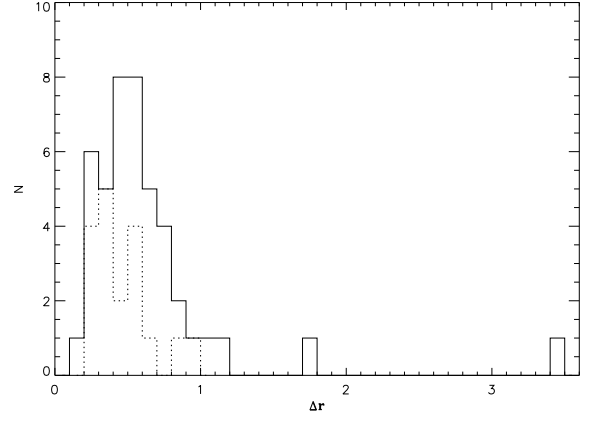


Fig. 8. The histogram of Δr for SSRQs and FSRQs in Gu & Ai (2011) and in this work. The dotted lines are for 18 SSRQs, and solid lines are for 44 FSRQs.

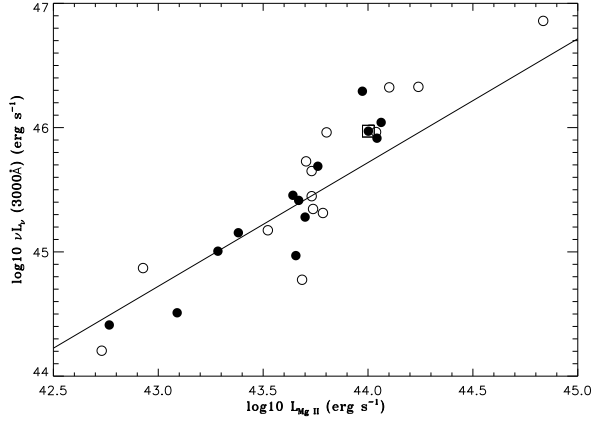


Fig. 6. The plot of broad Mg II line luminosity and continuum luminosity at 3000 Å for 13 SSRQs and 14 FSRQs. The symbols are same as in Fig. 4. The square is for BALQ SDSS J024534.07+010813.7. The solid line is the OLS bisector linear fit to radio-quiet AGNs in Kong et al. (2006), $\lambda L_{\lambda \text{ 3000\AA}} = 78.5 L_{\text{Mg II}}^{0.996}$.

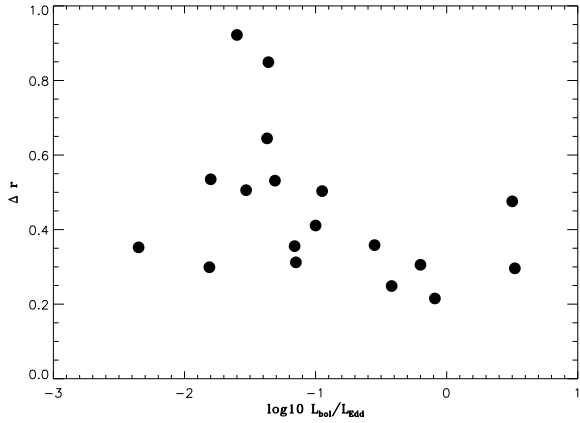


Fig. 7. The Eddington ratio versus the variability at r band Δr for SSRQs.

Table 1. Source list: Col. 1 - SDSS source name; Col. 2 - redshift; Col. 3 - radio loudness; Col. 4 - the spectral index between 1.4 and 4.85 GHz, of which GB6 flux density is used for those labeled with ^a, otherwise PMN one is used; Col. 5 - black hole mass in unit of solar mass; Col. 6 - disc bolometric luminosity in unit of erg s⁻¹; Col. 7 - the Eddington ratio $l = L_{\text{BOL}}/L_{\text{EDD}}$; Col. 8 - overall variation in r band; Col. 9 - the range of variation in the spectral index α_r ; Cols. (10-11) - the Spearman correlation coefficient and probability level, respectively.

SDSS source	z	$\log 10(R)$	α_r	$\log 10(M_{\text{BH}})$	$\log 10(L_{\text{BOL}})$	$\log 10(l)$	Δr	$\Delta \alpha_r$	r_s	prob.
(1)	(2)	(3)	(4)	(5)	(6)	(7)	(8)	(9)	(10)	(11)
SSRQs										
J000622.60-000424.4	1.0377	5.00	0.77	8.92	45.87	-1.16	0.35	0.28,1.00	0.146	0.24
J005905.51+000651.6	0.7189	3.71	0.50	8.96	45.92	-1.15	0.31	-0.16,0.49	0.315	1.32e-02
J013352.66+011345.1	0.3081	1.80	0.54 ^a	8.34	45.10	-1.35
J013514.39-000703.8	0.6712	3.73	0.75	8.41	44.92	-1.60	0.92	0.36,1.30	0.686	7.08e-10
J015509.00+011522.5	1.5480	2.99	0.51 ^a	8.64	46.55	-0.20	0.30	0.46,0.84	0.391	7.44e-04
J021225.56+010056.1	0.5128	2.56	0.55 ^a	8.77	45.51	-1.37	0.64	-0.08,0.28	0.275	0.03
J023313.81-001215.4	0.8072	2.93	0.78	8.41	45.57	-0.95	0.50	0.06,0.54	0.282	1.10e-02
J024534.07+010813.7	1.5363	3.16	1.10 ^a	9.65	45.95	-1.81	0.29	1.59,2.03	0.435	5.08e-04
J213004.75-010244.4	0.7040	3.25	0.79	10.08	45.85	-2.35	0.35	0.45,0.97	0.052	0.60
J213513.10-005243.8	1.6548	2.74	1.00	8.58	46.60	-0.09	0.22	0.40,0.77	0.279	0.02
J221409.96+005227.0	0.9078	2.87	0.77 ^a	9.05	45.86	-1.31	0.53	-0.09,0.43	0.405	1.94e-03
J231607.25+010012.9	2.6291	2.56	0.82 ^a	9.15	46.84	-0.42	0.24	0.38,0.89	0.445	8.31e-04
J233624.04+000246.0	1.0949	2.67	0.58	9.16	46.28	-1.00	0.41	0.12,0.61	0.787	1.37e-10
J235156.12-010913.3	0.1739	2.81	0.68	8.90	45.48	-1.53	0.50	-0.13,0.31	0.090	0.54
SSRQs from Gu & Ai (2011)										
J012401.76+003500.9	1.8516	3.85	0.86 ^a	9.36	46.11	-1.36	0.84	-0.52,0.61	0.687	6.8e-07
J012517.14-001828.9	2.2780	3.44	0.59	8.50	47.13	0.52	0.29	0.22,0.87	-0.202	0.11
J015832.51-004238.2	2.6071	3.58	0.87	8.29	46.90	0.50	0.47	0.44,1.19	-0.207	0.28
J021728.62-005227.2	2.4621	3.29	0.75	8.84	46.40	-0.55	0.35	0.45,1.28	0.488	7.7e-06
J022508.07+001707.2	0.5270	3.81	0.86 ^a	8.88	45.19	-1.80	0.53	0.25,0.68	0.470	0.03
FSRQs										
J000111.19-002011.5	0.5179	2.58	0.15	8.57	45.16	-1.52	0.36	0.64,1.04	0.426	5.44e-03
J010033.50+002200.1	0.7534	1.94	0.11 ^a	9.21	45.93	-1.40	0.55	-0.33,0.26	0.615	2.39e-08
J010826.84-003724.2	1.3724	3.31	0.26	8.76	46.31	-0.56	0.65	0.25,0.80	0.330	4.00e-03
J015105.80-003426.4	0.3352	1.55	-0.24	8.73	44.82	-2.03	0.55	0.05,0.95	0.807	2.39e-12
J020234.32+000301.7	0.3664	3.26	0.31	8.47	44.81	-1.77	0.18	0.19,0.58	-0.274	0.36
J020326.98+003744.3	1.5840	3.43	0.30 ^a	8.44	46.31	-0.24	0.80	0.24,0.89	0.678	2.71e-05
J021612.20-010518.9	1.4931	2.61	0.03	8.77	46.45	-0.43	0.27	0.37,0.73	0.263	0.04
J024854.81+001053.8	1.1457	2.92	0.30	8.65	46.00	-0.77	0.97	-0.31,0.56	0.723	7.06e-12
J025928.51-001959.9	2.0001	2.54	-0.63	8.87	47.29	0.30	0.30	0.08,0.66	0.323	1.24e-02
J031318.66+003623.9	1.2561	2.35	0.11 ^a	9.56	46.02	-1.65	0.32	0.52,0.98	0.353	4.51e-03
J220719.77+004157.3	1.8926	3.36	-0.05	8.85	45.90	-1.06	0.59	0.05,0.58	-0.171	0.18
J222729.05+000521.9	1.5133	3.02	0.15	9.19	46.52	-0.79	0.70	0.46,1.36	0.722	3.18e-10
J233200.00+011510.9	1.6395	3.45	0.27 ^a	8.75	46.01	-0.86	0.44	0.15,0.87	0.647	8.97e-08
J234624.56+001914.2	1.7775	2.84	-0.02 ^a	8.87	46.39	-0.60	0.79	0.09,0.72	0.702	9.77e-11
J234830.98+011037.6	1.7064	3.54	0.19 ^a	8.44	45.87	-0.68	0.60	0.17,1.08	0.746	1.67e-07